Journal of Electroanalytical Chemistry 879 (2020) 114782

Contents lists available at ScienceDirect

Journal of Electroanalytical Chemistry

journal homepage: www.elsevier.com/locate/jelechem

Chronopotentiometric study on the simultaneous transport of EDTA ionic species and hydroxyl ions through an anion-exchange membrane for electrodialysis applications

Kayo Santana Barros [a,b,*], Manuel César Martí-Calatayud [b], Emma M. Ortega [b], Valentín Pérez-Herranz [b], Denise Crocce Romano Espinosa [a]

[a] Department of Chemical Engineering, University of São Paulo (USP). Av. Professor Lineu Prestes, 580, Bloco 18 – Conjunto das Químicas, 05434-070 São Paulo, SP, Brazil
[b] IEC Group, ISIRYM, Universitat Politècnica de València – Spain, Camí de Vera s/n, 46022, P.O. Box 22012, València E-46071, Spain

ARTICLE INFO

Article history:
Received 13 July 2020
Received in revised form 15 October 2020
Accepted 16 October 2020
Available online 20 October 2020

Keywords:
Ethylenediaminetetraacetic acid
Ampholyte
Chronopotentiometry
Ion-exchange membrane
Electroconvection
Overlimiting phenomena

ABSTRACT

The use of EDTA as a complexing agent in electrodialysis has gained increasing attention in several industrial applications. Variations in pH at the membrane surface are known to alter the chemical equilibrium of EDTA species during electrodialysis. In this work, we investigate the simultaneous transport of EDTA species and hydroxyl ions through an anion-exchange membrane under alkaline conditions, and the influence of their relative concentrations on relevant membrane transport properties. Chronopotentiometric and current-voltage curves were obtained using solutions at different pH and electrolyte concentrations. Intense oscillations in membrane potential drop and a reduction in membrane resistance over time were verified for the solution at pH 11, where $EDTA^{4-}$ and OH^- ions presented similar molar concentrations. While the intense oscillations can be associated with the onset of electroconvection, the reduction in membrane potential drop can be explained based on the alteration of the chemical equilibrium in the system. At an advanced stage of concentration polarization, the increased exclusion of protons in the membrane phase induces an equilibrium shift and the dissociation of $HEDTA^{3-}$ into $EDTA^{4-}$ and H^+ ions. The formed $EDTA^{4-}$ ions migrate to the enriched solution, while protons are released back to the diluting diffusion boundary layer, increasing the conductivity in this region. The equilibrium shift in the membrane/electrolyte system and intense electroconvection at the membrane surface were also noted with the solution at pH 12. When the concentrations of OH^- and EDTA species are similar, the equilibrium shift and the occurrence of overlimiting phenomena become more prominent.

1. Introduction

For decades, electrodialysis has been mostly used for producing drinking water from brackish water sources [1]. In recent years, it has been often tested in a variety of fields, such as the treatment of industrial [2–5] and municipal wastewaters [6,7], the food and pharmaceutical industries [8,9], and in the production of organic acids [10–13]. Regardless of the purpose of electrodialysis, organic acids are generally present in the solutions to be treated as a contaminant, a desired product or a complexing agent.

The use of ethylenediaminetetraacetic acid (EDTA) as a complexing agent in electrodialysis systems is fairly widespread for separating metals by exploiting their different stability constants. $EDTA^{4-}$ anions participate in speciation reactions with metal cations, giving rise to different complex ions. Depending on the affinity between $EDTA^{4-}$ anions and metal cations, species of different charge sign and valency can be present in solution, e.g. some metals are able to form complex species with positive, neutral, or negative charge. Thus, under the application of an electric field, the addition of EDTA and its ability to combine with various metals can favor their separation in different compartments of an electrodialysis unit. The pH value and the relative concentration of EDTA and metals will determine which metal is transported through the anion-exchange membrane, which one crosses the cation-exchange membrane, and which one remains in the feed compartment. Some examples of this particular application of EDTA is the separation of mixtures of nickel-cobalt [14], calcium-cadmium [15], copper-cadmium [16], silver-copper-zinc [17], silver-zinc [16] and lithium-cobalt [18]. The separation and recovery of metals has gained relevance, given the exhaustion of traditional sources and the environmental impacts associated with their exploitation and with the management of wastes. The introduction of clean technologies into new production and recycling routes would contribute to achieve a circular economy for these crucial materials. Electromembrane processes are called to play a key role in this context, especially in the separation and recovery of metals present

* Corresponding author.
E-mail addresses: kayobarros@usp.br, (K.S. Barros), mcmarti@iqn.upv.es, (M.C. Martí-Calatayud), eortega@iqn.upv.es, (E.M. Ortega), vperez@iqn.upv.es, (V. Pérez-Herranz), espinosa@usp.br. (D.C.R. Espinosa).

http://dx.doi.org/10.1016/j.jelechem.2020.114782

in wastes generated in mining and electroplating industries [4,19], as well as during the treatment of waste from electrical and electronic equipment [20]. Frioui et al. [16] tested different complexing agents for separating metals by electrodialysis and verified that among the ligands, EDTA showed to be the best one in terms of charge modification of the metals and complex stability.

Recently, we evaluated the use of EDTA as a complexing agent in the brass electroplating industry [3] and the treatment, by electrodialysis, of the wastewater generated in this process [21,22]. We also investigated, by chronopotentiometry, the transport properties of EDTA-copper(II) and EDTA-zinc(II) complexes through an anion-exchange membrane [23]. However, in the previous works, SO_4^{2-} ions were also present at high concentrations and the influence of the relative concentration of OH^- and $EDTA^{4-}$ on the transport properties of the EDTA species through the membrane was not assessed in depth. This evaluation is quite important due to the dynamic behavior of pH and ion concentration in electrodialysis systems, especially at the surface of membranes, where some ions are intensively transferred while others are retained. According to Aouad et al. [24], evaluating the effects of complexing agents on the ion transport is crucial since the transfer of ions through the membranes is strongly affected by the concentration of the ligands and the solution pH. This is especially interesting for solutions with EDTA because the ionic species in equilibrium strongly depend on the solution pH, as shown in the dissociation reactions of Eq. (1)–(4) [18].

$$H_4EDTA \leftrightarrow H^+ + H_3EDTA^- \quad K_1 = 1.02 \times 10^{-2} \tag{1}$$

$$H_3EDTA^- \leftrightarrow H^+ + H_2EDTA^{2-} \quad K_2 = 2.14 \times 10^{-3} \tag{2}$$

$$H_2EDTA^{2-} \leftrightarrow H^+ + HEDTA^{3-} \quad K_3 = 6.92 \times 10^{-7} \tag{3}$$

$$HEDTA^{3-} \leftrightarrow H^+ + EDTA^{4-} \quad K_4 = 5.50 \times 10^{-11} \tag{4}$$

It is also known that the presence of weak electrolytes in electrodialysis can modify the ionic transport and affect the membrane properties [25,26]. For example, at two well separated pH levels, equilibrium reactions such as those presented in Eqs. (1)–(4) will imply that the ions which predominate in solution are different, each of them also differing in ionic mobility and charge. Ionic mobility of the prevailing counter-ion will influence the voltage drop through an ion-exchange membrane system. Besides this, the valency of the counter-ion plays an important role on its affinity toward the membrane fixed charges, thus affecting the membrane selectivity at the given experimental conditions. For this reason, it is of key importance to evaluate the effect of solution pH and complexing agent concentration on the performance of electromembrane processes in order to operate them under optimum conditions. To this end, methods of dynamic characterization of membranes, such as chronopotentiometry, cyclic voltammetry, impedance spectroscopy and current sweeps may be used [27].

Chronopotentiometry is an electrochemical method widely used to investigate transport properties and reactions that occur in membrane/electrolyte systems [28–30]. Chronopotentiometry reveals information regarding the dynamic response of membrane systems under different regimes. Thus, the potential of this technique lies on the fact that, it can be applied to track the evolution of distinct phenomena contributing to the overall membrane potential drop. Current-voltage curves at steady-state conditions can also be obtained from chronopotentiograms; therefore, important properties of the membrane/electrolyte system can also be determined using this technique [31]. Both chronopotentiometric and current-voltage curves provide information on the transport competition between ions. Chronopotentiometry has also been frequently used to evaluate overlimiting mass transfer phenomena that occur when the membrane/electrolyte system operates under intense concentration polarization, such as electroconvection, gravitational convection, and water dissociation [32–34].

The present work aims at evaluating, by chronopotentiometry, the influence of the simultaneous transport of hydroxyl ions and EDTA species present in a solution to be treated by electrodialysis. In contrast with previous studies, in this investigation, both OH^- and $EDTA^{4-}$ are the main anionic species present in solution, while monovalent Na^+ ions are the main cationic species. Current-voltage curves (CVC) and chronopotentiograms were obtained using solutions of EDTA at concentrations of 1.5×10^{-4}, 1.5×10^{-3}, 1.5×10^{-2} mol·L^{-1} and pH values of 9, 10, 11 and 12. Limiting current densities, ohmic resistances, plateau lengths and transition times were determined. The occurrence of overlimiting phenomena was assessed from the chronopotentiometric responses obtained at different levels of current density.

2. Materials and methods

2.1. Working solutions

Chronopotentiograms and current-voltage curves were obtained for solutions in different conditions of pH and EDTA concentration. The solutions were prepared with distilled water, EDTA disodium salt and NaOH. The chemicals were of analytical grade. For the evaluation of pH, 1.5×10^{-3} mol·L^{-1} EDTA solutions at pH 9, 10, 11 and 12 were tested, where the pH was adjusted by adding NaOH. For the evaluation of the initial EDTA concentration, solutions in 1.5×10^{-4} mol·L^{-1}, 1.5×10^{-3} mol·L^{-1} and 1.5×10^{-2} mol·L^{-1} at the same pH value of 11 were tested, where the pH was also adjusted by adding NaOH. The chemical composition of the evaluated solutions was based on typical values of EDTA concentration and pH of wastewaters generated in the electroplating industry [21,23].

2.2. Ion-exchange membranes

The anion-exchange membrane (AEM) evaluated was the HDX200, which contains quaternary amine groups attached to its matrix. The HDX100 membrane contains sulfonic acid as fixed groups and was used as the auxiliary cation-exchange membrane (CEM). Both membranes are commercial, heterogeneous and were supplied by Hidrodex. The characteristics of the HDX100 and HDX200 membranes are presented in Table 1 [22].

2.3. Electrochemical cell and chronopotentiometric measurements

The experiments were conducted using a three-compartment cell with a cation- and an anion-exchange membrane separating the central compartment from the cathode and anode, respectively. Two electrodes made of graphite were placed at the side compartments of the cell. The electric current was imposed by a potentiostat/galvanostat (Autolab, PGSTAT 30). The potential drop across the anion-exchange membrane was measured by two Ag/AgCl reference electrodes immersed in Luggin capillaries,

Table 1
Main characteristics of HDX 100 and HDX 200 membranes provided by the supplier.

Parameter	HDX100	HDX200	Unit
Ion group attached	$-SO_3^-$	$-NR_3^+$	–
Thickness	450	450	μm
Water content	35–50	30–45	%
Ion exchange capacity	≥ 2.0	≥ 1.8	mol·kg^{-1} (dry)
Surface resistance (measured in 0.1 mol·L^{-1} NaCl)	≤ 20	≤ 20	Ohm·cm^2
Permeselectivity (0.1 mol·L^{-1} KCl/0.2 mol·L^{-1} KCl)	≥ 90	≥ 89	%
Burst strength	≥ 06	≥ 0.6	MPa
Dimensional change rate	≤ 2	≤ 2	%
Water permeability	≤ 0.1 (< 0.2 MPa)	≤ 0.2 (< 0.035 MPa)	mL·h·cm^{-2}

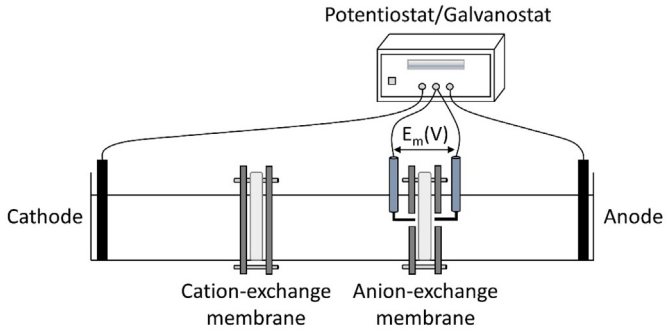

Fig. 1. A schematic representation of the chronopotentiometric setup.

installed at each side of the AEM. A schematic representation of the experimental setup is shown in Fig. 1. The effective area of the evaluated membranes was 1 cm^2 and before the tests, they were equilibrated for 24 h in the same solution to be tested subsequently. All the experiments were conducted in duplicate, at room temperature and without stirring. The estimated relative error between the values of the properties calculated from the current-voltage curves was below 5%. The chronopotentiograms were registered by applying current pulses for 300 s. Then, the current was interrupted, and the relaxation was allowed for 100 s before the application of the next pulse. The current–voltage curves were obtained from the steady-state potential drop across the anion-exchange membrane (E_m) corresponding to each applied current density.

2.4. Determination of the transport properties of the membrane/electrolyte system

A typical current-voltage curve can be divided into three regions, as represented in Fig. 2. The limiting current density (i_{lim}) was determined by the intersection of the tangential lines of the first and second regions of the curve, whereas the ohmic resistance (R_{ohm}) was determined from the inverse of the slope (α) of the tangential line of region I. The plateau length was estimated by the subtraction of the potential drops corresponding to the intersection between the tangential lines of regions II + III and the tangential lines of regions I + II. Transition times (τ) were obtained from the maximum of the derivative of the membrane potential drop with respect to time, which corresponds to the inflection in the chronopotentiograms [35], as represented in Fig. 3.

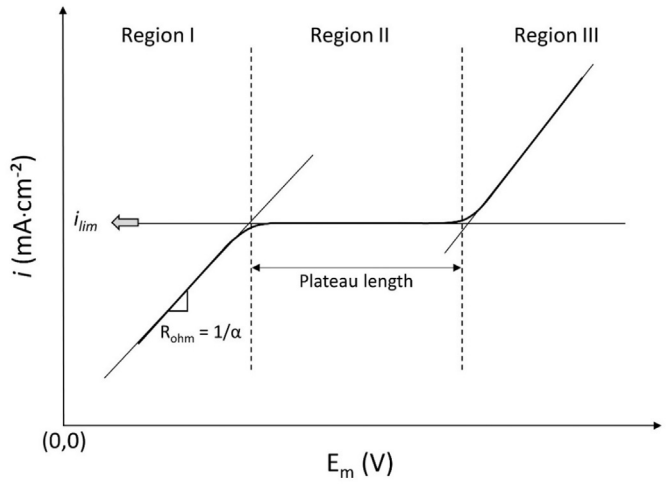

Fig. 2. Representation of a typical current-voltage curve.

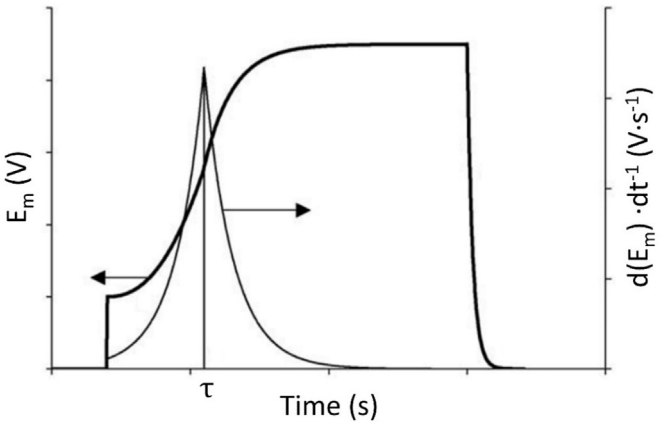

Fig. 3. Representation of a typical chronopotentiometric and derivative curves (adapted from ref. [27]).

3. Results and discussion

3.1. Evaluation of EDTA solutions at different pH conditions

3.1.1. Chronopotentiometric curves

Chronopotentiometric curves were obtained using 1.5×10^{-3} mol·L^{-1} EDTA solutions at pH values of 9, 10, 11 and 12. Fig. 4(a–d) present some chronopotentiograms obtained for each solution, whereas Fig. 4 (e, f) present some derivative curves constructed for the determination of transition times, τ. The derivative curves were obtained for each applied current density, although in Fig. 4(e, f) it is only shown for one current pulse. The values of transition times will be shown in this section.

For the solution at pH 9, typical chronopotentiograms (Fig. 4a) of a monopolar membrane were obtained, with a clear inflection point related to the occurrence of intense concentration polarization appearing at currents exceeding the limiting current density (i_{lim}). After the inflection point, the steady-state condition is reached and the membrane potential drop levels off. In this section of the curves, subtle oscillations in the potential drop were verified. A single transition time was obtained for each applied current density (Fig. 4e), which means that competition between species crossing the anion-exchange membrane is not significant. This can be supported by looking at the speciation diagrams constructed using Eqs. (1)–(4) (Fig. 5) and considering the fractions of existing anion species in solution. Na^+ ions were not added to the diagrams since they are co-ions that, in theory, do not migrate across the anion-exchange membrane. Note in Fig. 5 that at pH 9, the concentration of $HEDTA^{3-}$ in solution is considerably higher than the concentration of other species. In this case, the concentration of OH^- ions was not sufficiently high to alter the chemical equilibrium in the membrane system significantly. Features typically associated with overlimiting phenomena are not very notorious. Thus, it seems that none of such phenomena, such as electroconvection, gravitational convection and water dissociation, predominate over the other in the overlimiting regime.

For the solution at pH 10, the chronopotentiograms (Fig. 4b) were similar to the curves obtained at pH 9: a single transition time was observed for each current density (Fig. 4e) without additional inflection points. This was expected since the concentration of $HEDTA^{3-}$ ions in the electrolyte was higher than for other anionic species (Fig. 5). Hence, the competition between ions to be transferred through the membrane is still limited. It also appears that none of the possible mechanisms of overlimiting current transfer predominate over the others with this solution.

For the solution at pH 11, unexpected responses were registered in the chronopotentiograms (Fig. 4c), especially at currents above the limiting one. The potential drop showed a decrease after reaching an initial maximum as a consequence of intense concentration polarization (see 1.0 mA·cm^{-2}). Moreover, the registration of the maximum in potential

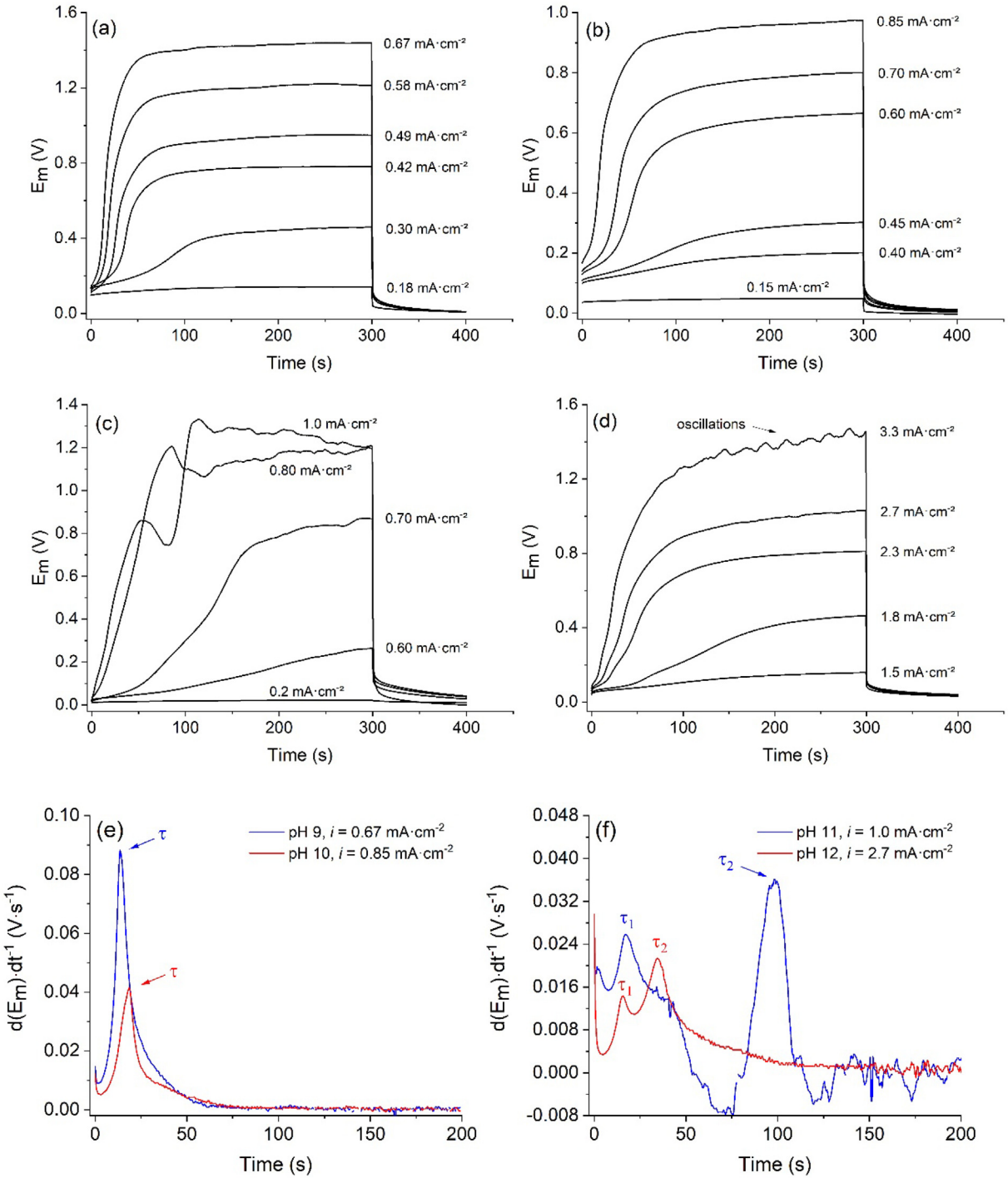

Fig. 4. Chronopotentiograms registered for solutions with EDTA in 1.5 × 10^{-3} mol·L^{-1} at pH (a) 9, (b) 10, (c) 11, and (d) 12. Figures (e,f) show the derivative of the membrane potential drop with respect to time obtained for the solutions at pH 9, 10, 11 and 12.

drop was accompanied by the development of noticeable oscillations over time. Two inflection points associated with distinct transition times were obtained for each current density, as shown for 1.0 mA·cm^{-2} in Fig. 4f. Similar features were manifested for several applied current densities and have been identified in previous studies as distinctive of various overlimiting phenomena [36]. The manifestation of distinct features in the chronopotentiograms points to the simultaneous development of both electroconvection and changes in the distribution of EDTA species in the electrolyte.

The initial maximum and subsequent reduction in potential drop can be explained by the alteration of the chemical equilibrium in the membrane/electrolyte system as OH^- ions are preferentially transferred through the membrane. The strong influence of pH changes in membrane systems with ampholyte solutions on chronopotentiograms and current-voltage curves was demonstrated via experimental and modeling studies conducted with monosodium phosphate solutions [25,37,38]. In those studies, the authors showed that when the membrane system is operated in underlimiting current regimes with an electrolyte at pH 4.7, the main current carriers are $H_2PO_4^-$ species. As the current density increases, the first i_{lim} is reached due to the saturation of the diffusion transport of the $H_2PO_4^-$ ions from the bulk solution to the membrane surface. The decrease in concentration at the membrane surface enhances the Donnan exclusion of protons from it, which leads to an increase in the pH inside the membrane. This shift in

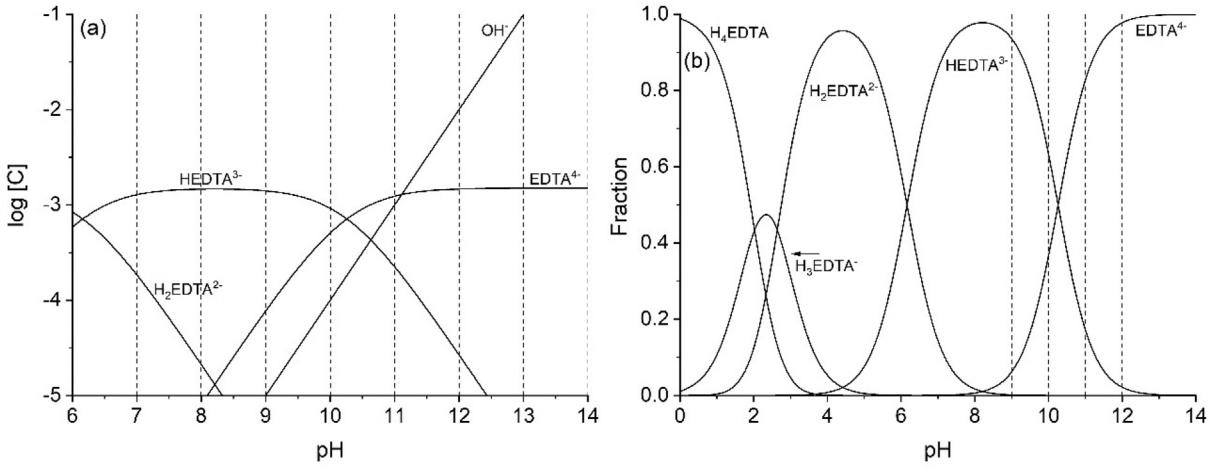

Fig. 5. Speciation diagrams shown as (a) log [C] and (b) fraction of ionic species versus pH constructed for 1.5×10^{-3} mol·L^{-1} EDTA solution. The vertical/dashed lines indicate pH values.

pH in the membrane phase converts part of $H_2PO_4^-$ ions into HPO_4^{2-} ions, which get into the enriched solution. Since the electric field is very high at the membrane surface, the H^+ ions generated in this dissociation reaction migrate toward the depleted diffusion boundary layer (DBL). When the concentration of HPO_4^{2-} reaches its saturation in the membrane, the second i_{lim} appears. The conversion of ampholyte species into others and the rate of H^+ and OH^- formation in these reactions was recently studied by different authors [39,40] via electrochemical impedance spectroscopy and by registering current-voltage curves. The results present in the above-mentioned articles may be correlated to the membrane/electrolyte system with EDTA species evaluated in our work.

Note in Fig. 5 that in the solution at pH 11, the initial concentrations of OH^- and $EDTA^{4-}$ ions are almost the same. Therefore, at underlimiting currents, these species are transferred through the membrane simultaneously. As shown in refs. [25, 37, 39], the intense transfer of OH^- ions increases the Donnan exclusion of protons from the membrane and decreases the pH in the depleting DBL. When this occurs, the chemical equilibrium in the DBL tends to shift toward the formation of $HEDTA^{3-}$ ions, according to Eq. (4). Under this condition, OH^-, $HEDTA^{3-}$, and $EDTA^{4-}$ ions are transferred simultaneously. In turn, the intense transfer of OH^- ions leads to an increase of the pH inside the membrane if compared to the DBL [37,39]. This induces a shift in the equilibrium toward the formation of more $EDTA^{4-}$ ions in the membrane phase. The formed $EDTA^{4-}$ ions migrate to the enriched solution, whereas the protons resulting from the dissociation of $HEDTA^{3-}$ return to the depleted DBL [37]. When $HEDTA^{3-}$ ions are saturated in the DBL, the first transition time (τ_1) shown in Fig. 4f is achieved. As the current density increases, the membrane fixed charges become equilibrated with $EDTA^{4-}$. As a consequence of the high mobility of protons excluded from the membrane, and the higher charge of $EDTA^{4-}$ ions as compared to $HEDTA^{3-}$, the conductivity of the system increases, until $EDTA^{4-}$ become also depleted at the membrane surface; when this occurs, the second transition time (τ_2) is reached. Similar results were obtained by Belashova et al. [37] for phosphate anions. This would explain the appearance of two transition times for each current pulse and the reduction in potential drop after reaching an initial maximum (Fig. 4c). These characteristics of chronopotentiograms were responsible for atypical features in the overlimiting region of the current-voltage curves registered for the solution at pH 11, as will be shown in detail in Section 3.1.2.

As can be seen from the curves obtained at the highest values of current density in Fig. 4c and d, the outbreak of electroconvection brings the solution layer next to the diluate side of the membrane surface into motion in the form of chaotic vortices, which becomes noticeable when oscillations in membrane potential drop take place [41]. The effects of electroconvection on membrane/ampholyte-containing systems were recently showed by Rybalkina et al. [42] from the visualization of vortexes at the membrane surface. As suggested by Martí-Calatayud et al. [43], the coexistence of electrolytic reactions and electroconvection may indicate that both phenomena take place in different locations of the system, where dissociation reactions predominate in the membrane phase rather than in the diffusion boundary layer. According to the authors, this phenomenon occurs when the membrane is initially equilibrated with low-charged counter-ions and a shift in equilibrium transforms them into multiply-charged ions, thus increasing membrane conductivity and releasing additional ions into the depleting diffusion boundary layer.

Fig. 4d shows the chronopotentiograms obtained for the solution at pH 12. Two transition times were observed for all applied current densities above the limiting one, as exemplary shown for 2.7 mA·cm^{-2} in Fig. 4f. Similarly to the discussion presented for the solution at pH 11, this can be explained by the intense transfer of OH^- ions through the membrane and the resulting reduction in pH at the diluting DBL, as a consequence of the increased Donnan exclusion of protons from the membrane phase [25,37,39]. This may have led to the simultaneous transport of OH^-, $HEDTA^{3-}$, and $EDTA^{4-}$ ions through the DBL toward the membrane, since at pH between 10 and 11, these species present similar concentrations (Fig. 5). As will be shown in Section 3.1.2., the competitive transport of $HEDTA^{3-}$ and $EDTA^{4-}$ ions was also noted in the current-voltage curves obtained for the solution at pH 12 since two limiting current densities were verified. Chronopotentiometric curves with intense oscillations in the potential drop were also obtained, which indicates that electroconvection occurred in this system [41,42].

For all solutions mentioned, the transition time decreased as the current density increased, which means that the time required for the depletion of counter-ions in the diffusion boundary layer is lower at higher values of current density. This is in accordance with the Sand equation (Eq. (5)), where D is the electrolyte diffusion coefficient, C_0 is the concentration in the bulk, z_j is the charge of the counter-ion, $\overline{t_j}$ and t_j are the transport numbers of the counter-ion in the membrane phase and in the solution, respectively, i is the current density and F is the Faraday's constant [44].

$$\tau = \frac{\pi D}{4}\left(\frac{z_j F C_0}{\overline{t_j} - t_j}\right)^2 \left(\frac{1}{i^2}\right) \quad (5)$$

Fig. 6 presents the dependence of transition time on current density, represented in Sand's coordinates, obtained with the solutions at pH 9–12. For the construction of the curves, only transition times obtained under current densities at least 1.5 times higher than the limiting current density of the membrane/electrolyte system were considered, as suggested

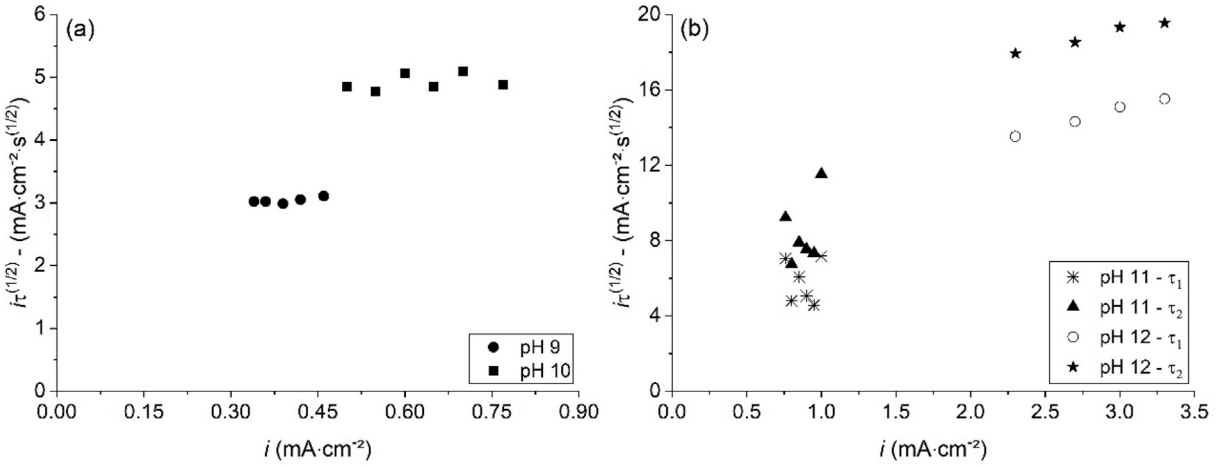

Fig. 6. Dependence of $i\tau^{1/2}$ on current density for the solutions at pH (a) 9, 10 and (b) 11, 12.

by Mareev et al. [45]. For the solutions at pH 9 and 10, a single transition time was obtained for each current pulse and the points are fairly constant, independent of the current density. The linearity of the plots points to the applicability of Sand equation for these solutions [46].

For the solution at pH 11, two transition times (τ_1 and τ_2) were obtained under all current densities above the limiting one, and none of them showed a linear behavior. The intense variability of $i\tau^{1/2}$ values as a function of i agrees with the chronopotentiometric curves suggesting intense

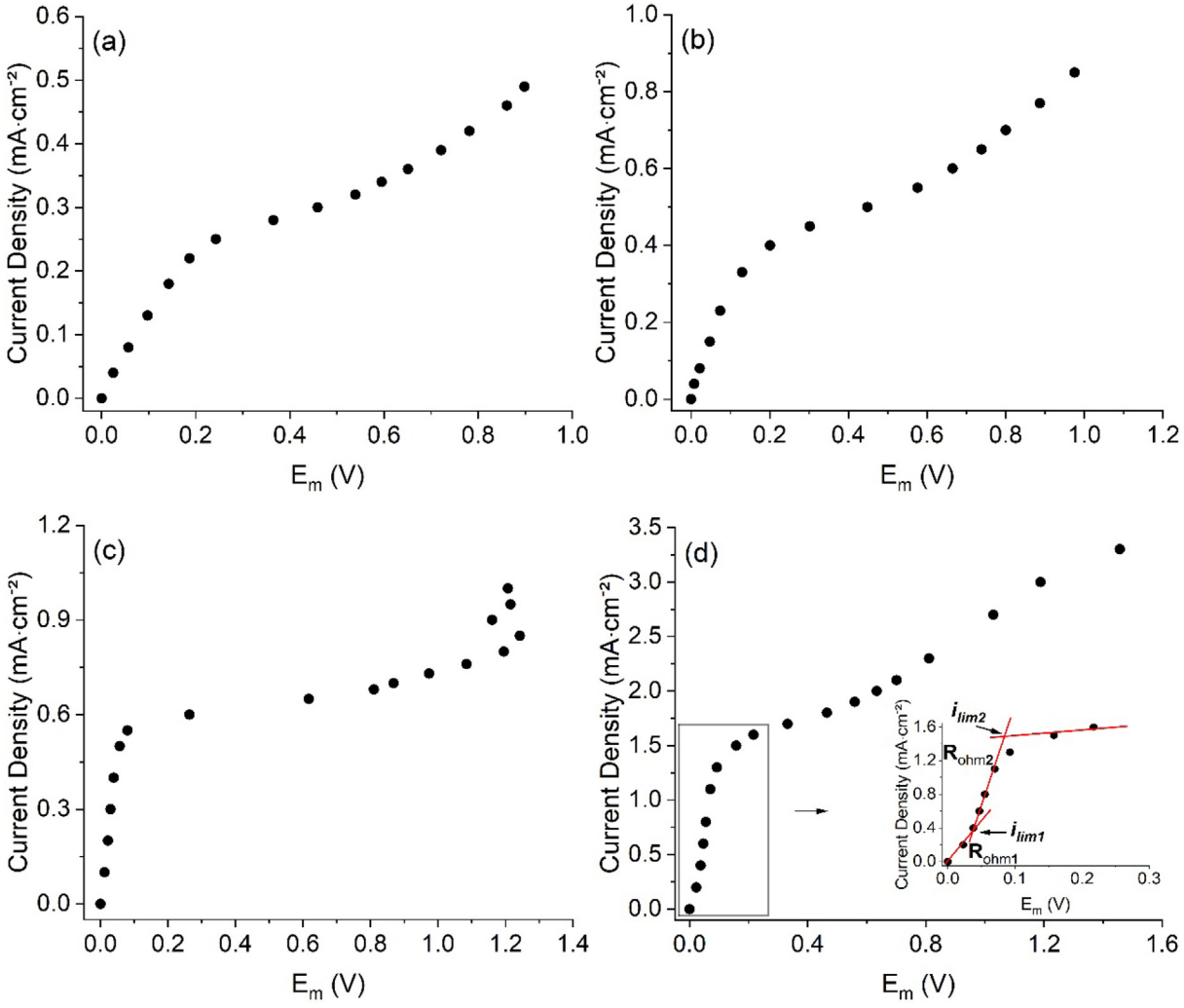

Fig. 7. Current-voltage curves constructed for 1.5×10^{-3} mol·L^{-1} EDTA solution at pH (a) 9, (b) 10, (c) 11, and (d) 12.

Table 2
Limiting current density, ohmic resistance and plateau length obtained for solutions with EDTA in 1.5 × 10^{-3} mol·L^{-1} at pH 9, 10, 11, and 12.

pH	9	10	11	12
Q_{eq}^{-} (meq·L^{-1})	4.6	5.1	6.8	16
i_{lim} (mA·cm^{-2})	0.24	0.34	0.51	i_{lim1}: 0.35; i_{lim2}: 1.48
R_{ohm} (Ω·cm^2)	833	333	110	R_{ohm1}: 96; R_{ohm2}: 46
Plateau length (V)	0.4	0.5	0.6	0.6

overlimiting phenomena for the solution at pH 11 (Fig. 4c). Thus, when the solution at pH 11 is used, overlimiting phenomena may control ion transfer through the membrane. In this membrane/electrolyte system, Sand equation is not applicable since it was deduced from the Nernst-Planck equation assuming a stagnant diffusion layer of infinite thickness near the membrane/electrode [47]. This means the equation does not consider convection phenomena experimentally observed for the solution at pH 11.

For the solution at pH 12, two transition times were also obtained for all applied current densities above the limiting one, as occurred for the solution at pH 11. However, in the case of pH 12, the curves of τ_1 and τ_2 follow a linear trend, where the $i\tau^{1/2}$ values increase with i. The increase in $i\tau^{1/2}$ indicates that, for this solution, ion transfer through the membrane is accompanied by chemical reactions such as protonation-deprotonation of EDTA species [46]. This is in accordance with the double transition times obtained at pH 12; each one was associated with the depletion of distinct species in the DBL, which were formed by chemical reactions in the membrane/electrolyte system.

Lastly, note in Fig. 6 that the greater the solution pH, the greater the $i\tau^{1/2}$ values. Eq. (5) indicates that this trend is correlated to changes in the transport number of counter-ions (EDTA species) in the membrane as the solution pH increased, since only the $\overline{t_j}$ term is affected by the pH variation. These results show that the increase in solution pH leads to a decrease in the transport number of EDTA species due to the competitive transport of these ions and OH^-.

3.1.2. Current-voltage curves

The current-voltage curves constructed for the solutions at pH values ranging from 9 to 12 are presented in Fig. 7.

The current-voltage curves obtained for the solutions at pH 9 and 10 (Fig. 7a and b, respectively) showed typical behaviors with three well defined regions. This is consistent with the chronopotentiograms obtained

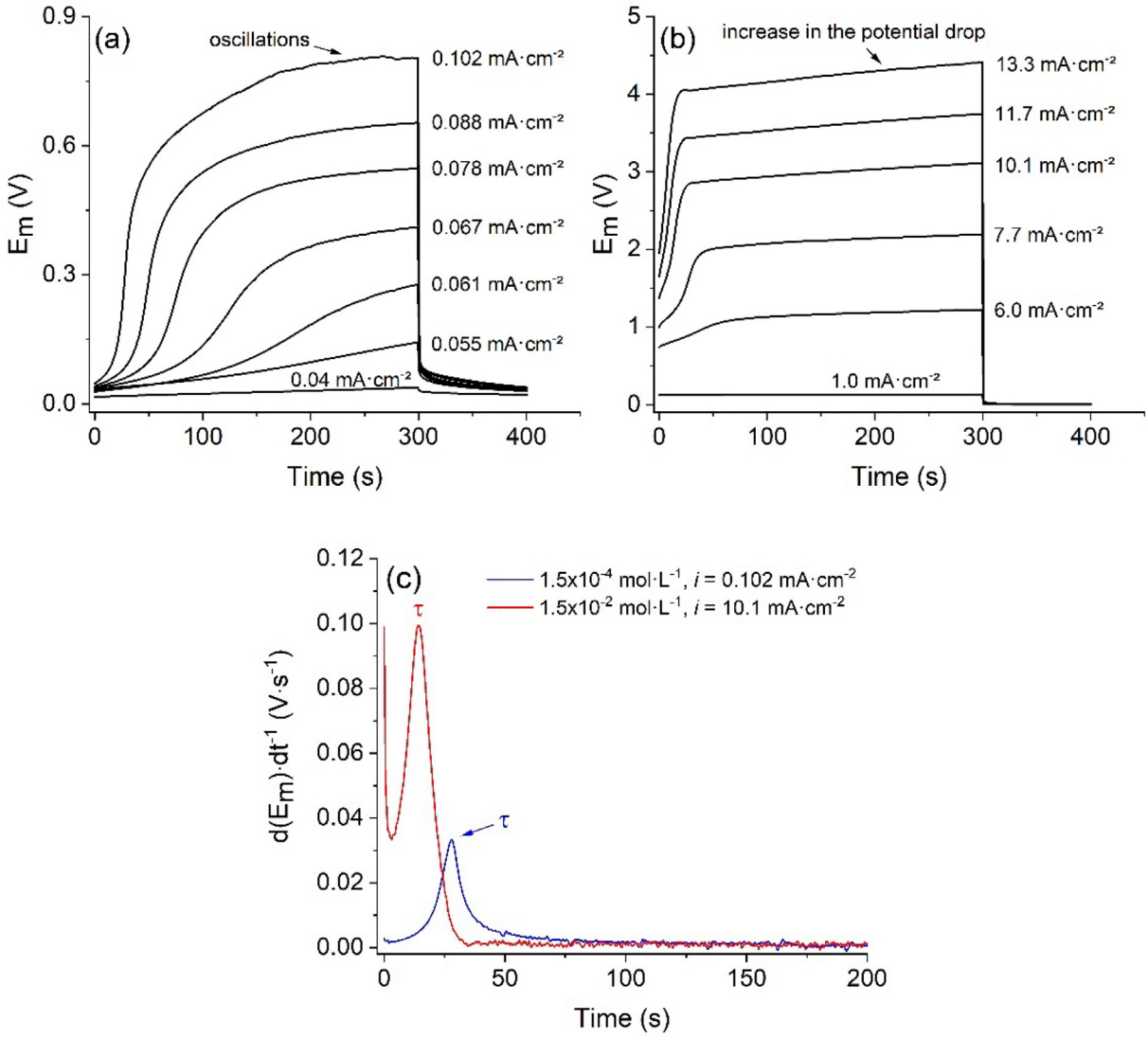

Fig. 8. Chronopotentiograms constructed for solutions at pH 11 and EDTA concentration of (a) 1.5 × 10^{-4} mol·L^{-1} and (b) 1.5 × 10^{-2} mol·L^{-1}. Figure (c) shows the derivative of the membrane potential drop with respect to time obtained for both solutions.

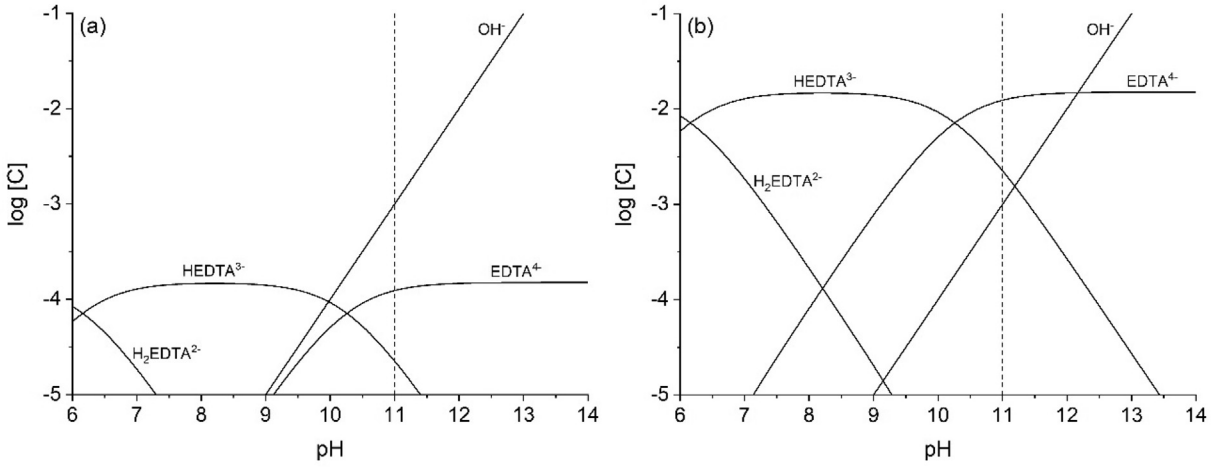

Fig. 9. Speciation diagram constructed for the solution at EDTA concentration of (a) 1.5×10^{-4} mol·L^{-1} and (b) 1.5×10^{-2} mol·L^{-1}. The vertical/dashed line indicates pH 11.

for these solutions. For the solution at pH 11 (Fig. 7c), the CVC showed a non-expected behavior since the potential drop decreased as the current density increased beyond ~0.85 mA·cm^{-2}. This is in accordance with the chronopotentiograms of this solution and may be explained by the formation of more conductive ions as the chemical equilibrium in the membrane phase was modified, as mentioned in Section 3.1.1.

For the solution at pH 12, the current-voltage curve (Fig. 7d) showed well defined regions, which agrees with the chronopotentiograms presented for this solution. Two limiting current densities (i_{lim1} and i_{lim2}) and two ohmic resistances (R_{ohm1} and R_{ohm2}) were verified since a change in the slope of the CVC occurred at 0.35 mA·cm^{-2} and then at 1.48 mA·cm^{-2}. This supports the discussion in Section 3.1.1 about the equilibrium shift taking place as a consequence of the Donnan exclusion of protons as OH^- ions were intensively transferred through the membrane. Thus, the pH reduction in the DBL may have led to the simultaneous transfer of OH^-, $HEDTA^{3-}$ and $EDTA^{4-}$ ions across the membrane. In this case, i_{lim1} and i_{lim2} must have appeared due to the depletion of $HEDTA^{3-}$ and $EDTA^{4-}$ ions, respectively, in the DBL. Note in Table 2 that R_{ohm2} is considerably lower than R_{ohm1}, which is explained by the reduction in the resistance of the depleted boundary solution as protons were excluded from the membrane phase [37]. Current-voltage curves showing two i_{lim} due to the shift in equilibrium as protons were excluded from the membrane were also verified with other ampholyte solutions [25,37,42].

The results of limiting current density, ohmic resistance and plateau length of each solution are shown in Table 2. The anionic equivalent charge (Q_{eq}^-) is also included in the table, which was determined by Eq. (6). In the equation, C_j and z_j are the concentration and the charge of a species j, respectively. For the use of Eq. (6), the concentrations of the main ionic species in equilibrium in each solution were determined from Fig. 5.

$$Q_{eq}^- = \sum |z_j| C_j \quad (6)$$

The limiting current density of the tested solutions increased with the solution pH. This behavior is consistent since the anionic equivalent charge also increased and the greater the concentration of ions in solution, the higher the current needed to achieve their depletion in the diffusion boundary layer [23]. As shown in Fig. 5, the solutions at each pH evaluated presented different predominant species, with different charges and mobilities. Therefore, the i_{lim} of the solutions at each pH correspond to the depletion of different species. The ohmic resistance showed an opposite behavior, which agrees with the increase in the solution conductivity with more $EDTA^{4-}$ and mainly OH^- ions (greater anionic equivalent charge) [48]. The increased Donnan exclusion of protons as the pH was increased may also be associated with the reduction in the ohmic resistance since the released protons reduce the resistance of the depleted boundary solution [37], as previously discussed. Lastly, the plateau length increased with the solution pH. This occurred since OH^- ions are transferred by the Grotthuss mechanism, carrying the charge by "tunnelling" from one water molecule to another without bringing liquid volume into motion; this hinders the onset of electroconvection and increases the plateau length [26,49].

3.2. Dilution and concentration of the solution at pH 11

3.2.1. Chronopotentiometric curves

Considering the behaviors of the curves obtained with the solution at pH 11, chronopotentiograms and CVCs were constructed for solutions at the same pH and different concentrations of EDTA: 10 times more diluted (1.5×10^{-4} mol·L^{-1}) and 10 times more concentrated (1.5×10^{-2} mol·L^{-1}). Fig. 8(a, b) show some chronopotentiograms obtained for both solutions, whereas Fig. 8(c) shows derivative curves constructed for the determination of transition times.

For the diluted solution (Fig. 8a), typical chronopotentiometric curves were obtained, without additional inflection points or intense reduction in the potential drop during the progress of concentration polarization.

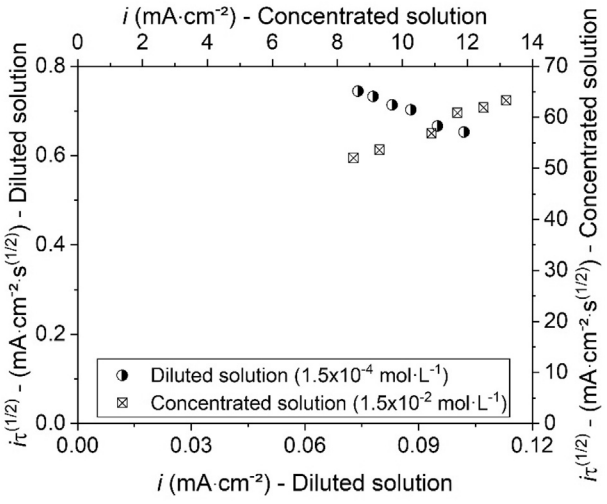

Fig. 10. Dependence of $i\tau^{1/2}$ on current density for the EDTA solutions in 1.5×10^{-4} mol·L^{-1} and 1.5×10^{-2} mol·L^{-1}.

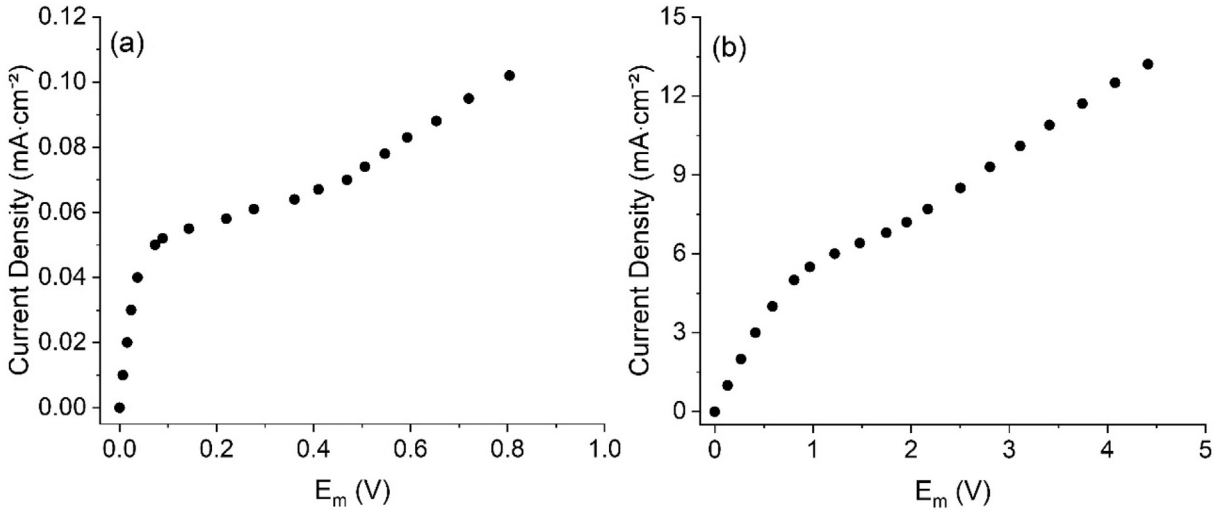

Fig. 11. Current-voltage curves constructed for solutions at pH 11 and EDTA concentration of (a) 1.5×10^{-4} mol·L^{-1} and (b) 1.5×10^{-2} mol·L^{-1}.

Speciation diagrams for the anionic species were constructed with the chemical composition of the most diluted and concentrated solutions (Fig. 9). Note that the concentration of OH^- ions in the diluted solution was much greater than the $HEDTA^{3-}$ and $EDTA^{4-}$ species (Fig. 9a). Since hydroxyl ions presented greater concentrations, they are assumed to be the main charge carriers through the membrane. A single transition time was obtained for each applied current density (Fig. 8c), which confirms that OH^- ions and the species from EDTA did not compete intensively to cross the membrane. Oscillations in the potential drop were verified for the highest values of applied current density, as shown for the curve obtained at 0.102 mA·cm^{-2}. This is a typical feature of electroconvection that was not verified for the concentrated solution under any current density (Fig. 8b). These results agree with previous investigations, where it is reported that electroconvection occurs more intensively in more diluted solutions as a consequence of the thicker space charge region developed near the membrane surface [41,50,51]. These results also agree with the plateau length of the current-voltage curves, as will be shown in Section 3.2.2.

For the concentrated solution (Fig. 8b), typical chronopotentiograms were also obtained, without additional inflection points, and with a single transition time for each applied current density (Fig. 8c). In this case, the considerably greater concentrations of the EDTA species, especially $EDTA^{4-}$ ions, as compared to OH^- ions in solution hindered the alteration of the chemical equilibrium. A continuous increase in the potential drop was verified after the sharp increase corresponding to the transition time, when the potential drop was expected to be constant over time (as indicated in Fig. 8b for 13.3 mA·cm^{-2}). This may be explained by the preferential transport of EDTA species rather than OH^- ions since the former species present lower diffusion/mobility coefficient than OH^- ions. It is worth mentioning that if the current applications had lasted considerably longer times with the concentrated solution, a second transition time could have been observed, as occurred in ref. [38] using NaH_2PO_4 solution in 0.02 mol·L^{-1}.

Fig. 10 presents the dependence of transition time on current density, represented in Sand's coordinates, obtained for the EDTA solutions at pH 11 in 1.5×10^{-4} mol·L^{-1} and 1.5×10^{-2} mol·L^{-1}. In both cases, a single transition time was obtained for each current pulse and τ followed a linear trend, but with different slopes. As mentioned in Section 3.1.1., the appearance of a slope in the curve of $i\tau^{1/2}$ vs. i is related to chemical reactions taking place in the membrane/electrolyte system together with ion transfer. The curves exhibit different slopes (negative for the diluted solution and positive for the concentrated one) due to the different kinetics of the reactions that occur at each concentration [46]. This is associated with the differences in the predominant species in each solution, as shown in Fig. 9. For both concentrations, the unexpected oscillations shown for the solution in 1.5×10^{-3} mol·L^{-1} (Fig. 6b) were not verified with the most diluted and concentrated solutions. This agrees with the chronopotentiometric curves obtained for the solutions at pH 11 and different concentrations.

3.2.2. Current-voltage curves

The current-voltage curves constructed for the solutions at pH 11 in 1.5×10^{-4} mol·L^{-1} and 1.5×10^{-2} mol·L^{-1} are presented in Fig. 11.

The curves obtained for both solutions showed the three well defined regions, differently from that obtained for the solution in 1.5×10^{-3} mol·L^{-1}. Table 3 presents the results of limiting current density, ohmic resistance and plateau length for the solutions at pH 11 and different concentrations. The values of anionic equivalent charge of the solutions are also present in the table, which were determined using the concentrations of species from the speciation diagrams shown in Fig. 5 and 9.

The increase in the limiting current density with concentration showed a linear behavior. This may be explained by the linear increase of $EDTA^{4-}$ species, which was the predominant species in the three solutions at pH 11 evaluated (Figs. 5a and 9). Therefore, the increase in i_{lim} of the solutions at each EDTA concentration corresponds mainly to the increase of $EDTA^{4-}$ species. In this case, the proportional increase of i_{lim} and EDTA concentration is in agreement with the classical concentration polarization theory expressed by Eq. (7) [52]. In the equation, δ is the boundary layer thickness and the other terms are the same as those presented in Eq. (5). Lastly, the plateau length increased with the solution concentration, which means that electroconvection tends to occur more intensively in the diluted solution. The plateau length corresponds to a transition zone between the first and third regions of the current-voltage curve. Hence, it represents the membrane potential drop that must be surpassed to change

Table 3
Limiting current density, ohmic resistance and plateau length obtained for solutions with EDTA at pH 11 in 1.5×10^{-4}, 1.5×10^{-3} and 1.5×10^{-2} mol·L^{-1}.

EDTA concentration (mol·L^{-1})	$1.5{\cdot}10^{-4}$	$1.5{\cdot}10^{-3}$	$1.5{\cdot}10^{-2}$
Q_{eq}^{-} (meq·L^{-1})	1.6	6.8	58.7
i_{lim} (mA·cm^{-2})	0.051	0.51	5.1
R_{ohm} (Ω·cm^2)	833	110	133
Plateau length (V)	0.5	0.6	1.2

the main ionic transfer mechanism from diffusion and migration to overlimiting mechanisms, such as electroconvection, gravitational convection and water dissociation [53]. Therefore, the smaller plateau length registered for the most diluted solution indicates that the energy required to destroy the diffusion boundary layer and reactivate transport from the bulk toward the membrane surface is lower in this case [27,48]. Thus, electroconvection is favored at low concentrations, which agrees with the chronopotentiograms obtained for each solution and with the literature [41].

$$i_{lim} = \frac{zFC_0D}{\delta(\overline{t_i} - t_i)} \quad (7)$$

4. Conclusions

Chronopotentiometric and current-voltage curves were obtained with 1.5×10^{-3} mol·L^{-1} EDTA solutions at pH 9, 10, 11 and 12. The curves for solutions at pH 9 and 10 showed typical shapes with well-defined regions. A single transition time was obtained for each current pulse and features typically associated with overlimiting phenomena were not very notorious. In these solutions, the concentration of $HEDTA^{3-}$ ions was higher than the concentration of OH^-, which explains the small influence of the simultaneous transport of these species through the membrane on the curves obtained.

For the solution at pH 11, where the concentrations of OH^- and $EDTA^{4-}$ ions were almost the same, all chronopotentiograms registered at current densities above the limiting one showed unexpected behaviors: intense oscillations in the membrane potential drop and a reduction in membrane resistance. Besides, two transition times were obtained for all current pulses. The findings indicate that these features appeared due to a shift in the chemical equilibrium occurring in the membrane/electrolyte system: the intense transfer of OH^- ions together with $EDTA^{4-}$ led to an intensification of the Donnan exclusion of protons from the membrane. Under this condition, the pH in the depleting DBL decreased and the equilibrium at the membrane surface was shifted toward the formation of $HEDTA^{3-}$ species. Thus, OH^-, $HEDTA^{3-}$, and $EDTA^{4-}$ ions were transferred simultaneously across the membrane. In turn, the pH inside the membrane increased, leading to an equilibrium shift in the membrane toward the formation of more $EDTA^{4-}$ ions. The $EDTA^{4-}$ ions migrated to the enriched solution, whereas the protons formed in the dissociation reaction of $HEDTA^{3-}$ returned to the depleted DBL. When $HEDTA^{3-}$ ions were saturated in the DBL, the first transition time was achieved. When $EDTA^{4-}$ ions became depleted at the membrane surface, the second transition time was reached. The intense transfer of OH^- and the formation of $EDTA^{4-}$ together with H^+ increased the membrane conductivity. Intense oscillations in the membrane potential drop indicate that electroconvection takes place simultaneously to the equilibrium shift, but at the membrane surface. Solutions 10 times more diluted (1.5×10^{-4} mol·L^{-1}) and 10 times more concentrated (1.5×10^{-2} mol·L^{-1}) at the same pH of 11 were also evaluated. Typical chronopotentiograms and current-voltage curves were obtained since the simultaneous transport of OH^- ions and EDTA species did not occur so intensively with any of these solutions.

For the solution at pH 12, two transition times were obtained for all applied current densities above the limiting one. Similarly to the solution at pH 11, this occurred due to the equilibrium shift in the membrane/electrolyte system, which led to the competitive transfer of OH^-, $HEDTA^{3-}$, and $EDTA^{4-}$ ions across the membrane. Intense oscillations associated with the occurrence of electroconvection at the membrane surface were verified in the curves. The two transition times obtained for each current pulse at pH 12 agreed with the current-voltage curve showing two limiting current densities and two ohmic resistances.

The limiting current density and the plateau length increased as the concentration and the pH of the solutions increased, whereas the ohmic resistance showed an opposite behavior. These results agree with the calculated values of anionic equivalent charge of each solution.

CRediT authorship contribution statement

Kayo Santana Barros: Conceptualization, Methodology, Validation, Data curation, Formal analysis, Investigation, Writing - original draft, Writing - review & editing, Visualization. **Manuel César Martí-Calatayud:** Writing - original draft, Writing - review & editing, Visualization. **Emma M. Ortega:** Conceptualization, Software, Data curation, Resources. **Valentín Pérez-Herranz:** Conceptualization, Methodology, Formal analysis, Data curation, Writing - review & editing, Project administration, Resources, Supervision. **Denise Crocce Romano Espinosa:** Funding acquisition, Project administration, Supervision.

Declaration of Competing Interest

The authors declare that they have no known competing financial interests or personal relationships that could have appeared to influence the work reported in this paper.

Acknowledgements

The authors gratefully acknowledge the financial support given by funding agencies CNPq (Process 141346/2016-7) and CAPES (Process 88881.190502/2018-01). This study was financed in part by the Coordenação de Aperfeiçoamento de Pessoal de Nível Superior - Brasil (CAPES) - Finance Code 001.

References

[1] R.K. Nagarale, G.S. Gohil, V.K. Shahi, Recent developments on ion-exchange membranes and electro-membrane processes, Adv. Colloid Interf. Sci. 119 (2006) 97–130, https://doi.org/10.1016/j.cis.2005.09.005.
[2] Y. Zheng, Z. Li, X. Wang, X. Gao, C. Gao, The treatment of cyanide from gold mine effluent by a novel five-compartment electrodialysis, Electrochim. Acta 169 (2015) 150–158, https://doi.org/10.1016/j.electacta.2015.04.015.
[3] K.S. Barros, E.M. Ortega, V. Pérez-Herranz, D.C.R. Espinosa, Evaluation of brass electrodeposition at RDE from cyanide-free bath using EDTA as a complexing agent, J. Electroanal. Chem. 865 (2020) 114129, https://doi.org/10.1016/j.jelechem.2020.114129.
[4] M.C. Martí-Calatayud, D.C. Buzzi, M. García-Gabaldón, E. Ortega, A.M. Bernardes, J.A.S. Tenório, V. Pérez-Herranz, Sulfuric acid recovery from acid mine drainage by means of electrodialysis, Desalination 343 (2014) 120–127, https://doi.org/10.1016/j.desal.2013.11.031.
[5] T. Scarazzato, K.S. Barros, T. Benvenuti, M.A. Siqueira Rodrigues, D.C. Romano Espinosa, A. Moura Bernardes, V. Pérez-Herranz, Achievements in Electrodialysis Processes for Wastewater and Water Treatment, Elsevier Inc., 2020 https://doi.org/10.1016/B978-0-12-817378-7.00005-7.
[6] C.R. Gally, T. Benvenuti, C.D.M. Da Trindade, M.A.S. Rodrigues, J. Zoppas-Ferreira, V. Pérez-Herranz, A.M. Bernardes, Electrodialysis for the tertiary treatment of municipal wastewater: efficiency of ion removal and ageing of ion exchange membranes, J. Environ. Chem. Eng. 6 (2018) 5855–5869, https://doi.org/10.1016/j.jece.2018.07.052.
[7] E.H. Rotta, C.S. Bitencourt, L. Marder, A.M. Bernardes, Phosphorus recovery from low phosphate-containing solution by electrodialysis, J. Membr. Sci. 573 (2019) 293–300, https://doi.org/10.1016/j.memsci.2018.12.020.
[8] D. Labbé, M. Araya-Farias, A. Tremblay, L. Bazinet, Electromigration feasibility of green tea catechins, J. Membr. Sci. 254 (2005) 101–109, https://doi.org/10.1016/j.memsci.2004.10.048.
[9] L. Yu, A. Lin, L. Zhang, C. Chen, W. Jiang, Application of electrodialysis to the production of vitamin C, Chem. Eng. J. 78 (2000) 153–157, https://doi.org/10.1016/S1385-8947(00)00136-4.
[10] J. Kaláb, Z. Palatý, Electrodialysis of oxalic acid: batch process modeling Jiří, Chem. Pap. 66 (2012) 1118–1123, https://doi.org/10.2478/s11696-012-0232-5.
[11] J.S.J. Ferrer, S. Laborie, G. Durand, M. Rakib, Formic acid regeneration by electromembrane processes, J. Membr. Sci. 280 (2006) 509–516, https://doi.org/10.1016/j.memsci.2006.02.012.
[12] M. Szczygiełda, K. Prochaska, Alpha-ketoglutaric acid production using electrodialysis with bipolar membrane, J. Membr. Sci. 536 (2017) 37–43, https://doi.org/10.1016/j.memsci.2017.04.059.
[13] K. Prochaska, M.J. Woźniak-Budych, Recovery of fumaric acid from fermentation broth using bipolar electrodialysis, J. Membr. Sci. 469 (2014) 428–435, https://doi.org/10.1016/j.memsci.2014.07.008.
[14] A.J. Chaudhary, J.D. Donaldson, S.M. Grimes, N.G. Yasri, Separation of nickel from cobalt using electrodialysis in the presence of EDTA, J. Appl. Electrochem. 30 (2000) 439–445, https://doi.org/10.1023/A:1003966132167.
[15] M. Kubal, T. Machula, N. Strnadová, Separation of calcium and cadmium by Electrodialysis in the presence of ethylenediaminetetraacetic acid, Sep. Sci. Technol. 33 (1998) 1969–1980, https://doi.org/10.1080/01496399808545040.

[16] S. Frioui, R. Oumeddour, S. Lacour, Highly selective extraction of metal ions from dilute solutions by hybrid electrodialysis technology, Sep. Purif. Technol. 174 (2017) 264–274, https://doi.org/10.1016/j.seppur.2016.10.028.
[17] A.T. Cherif, A. Elmidaoui, C. Gavach, Separation of Ag+, Zn2+ and Cu2+ ions by electrodialysis with monovalent cation specific membrane and EDTA, J. Membr. Sci. 76 (1993) 39–49, https://doi.org/10.1016/0376-7388(93)87003-T.
[18] A. Iizuka, Y. Yamashita, H. Nagasawa, A. Yamasaki, Y. Yanagisawa, Separation of lithium and cobalt from waste lithium-ion batteries via bipolar membrane electrodialysis coupled with chelation, Sep. Purif. Technol. 113 (2013) 33–41, https://doi.org/10.1016/j.seppur.2013.04.014.
[19] L. Marder, E.M. Ortega Navarro, V. Pérez-Herranz, A.M. Bernardes, J.Z. Ferreira, Chronopotentiometric study on the effect of boric acid in the nickel transport properties through a cation-exchange membrane, Desalination 249 (2009) 348–352, https://doi.org/10.1016/j.desal.2009.06.040.
[20] L. Zhang, Z. Xu, A review of current progress of recycling technologies for metals from waste electrical and electronic equipment, J. Clean. Prod. 127 (2016) 19–36, https://doi.org/10.1016/j.jclepro.2016.04.004.
[21] K.S. Barros, T. Scarazzato, V. Pérez-Herranz, D.C.R. Espinosa, Treatment of cyanide-free wastewater from brass electrodeposition with EDTA by electrodialysis: evaluation of underlimiting and overlimiting operations, Membranes (Basel) 10 (2020) 69, https://doi.org/10.3390/membranes10040069.
[22] K.S. Barros, M.C. Martí-Calatayud, V. Pérez-Herranz, D.C.R. Espinosa, A three-stage chemical cleaning of ion-exchange membranes used in the treatment by electrodialysis of wastewaters generated in brass electroplating industries, Desalination 492 (2020) 114628, https://doi.org/10.1016/j.desal.2020.114628.
[23] K.S. Barros, D.C.R. Espinosa, Chronopotentiometry of an anion-exchange membrane for treating a synthesized free-cyanide effluent from brass electrodeposition with EDTA as chelating agent, Sep. Purif. Technol. 201 (2018) 244–255, https://doi.org/10.1016/j.seppur.2018.03.013.
[24] F. Aouad, A. Lindheimer, M. Chaouki, C. Gavach, Loss of permselectivity of anion exchange membranes in contact with zinc chloride complexes, Desalination 121 (1999) 13–22, https://doi.org/10.1016/S0011-9164(99)00003-X.
[25] E.D. Melnikova, N.D. Pismenskaya, L. Bazinet, S. Mikhaylin, V.V. Nikonenko, Effect of ampholyte nature on current-voltage characteristic of anion-exchange membrane, Electrochim. Acta 285 (2018) 185–191, https://doi.org/10.1016/j.electacta.2018.07.186.
[26] C. Gally, M. García-Gabaldón, E.M. Ortega, A.M. Bernardes, V. Pérez-Herranz, Chronopotentiometric study of the transport of phosphoric acid anions through an anion-exchange membrane under different pH values, Sep. Purif. Technol. 238 (2020) 116421, https://doi.org/10.1016/j.seppur.2019.116421.
[27] L. Marder, E.M. Ortega Navarro, V. Perez-Herranz, A.M. Bernardes, J.Z. Ferreira, Evaluation of transition metals transport properties through a cation exchange membrane by chronopotentiometry, J. Membr. Sci. 284 (2006) 267–275, https://doi.org/10.1016/j.memsci.2006.07.039.
[28] D.Y. Butylskii, S.A. Mareev, N.D. Pismenskaya, P.Y. Apel, O.A. Polezhaeva, V.V. Nikonenko, Phenomenon of two transition times in chronopotentiometry of electrically inhomogeneous ion exchange membranes, Electrochim. Acta 273 (2018) 289–299, https://doi.org/10.1016/j.electacta.2018.04.026.
[29] S.A. Mareev, A.V. Nebavskiy, V.S. Nichka, M.K. Urtenov, V.V. Nikonenko, The nature of two transition times on chronopotentiograms of heterogeneous ion exchange membranes: 2D modelling, J. Membr. Sci. 575 (2019) 179–190, https://doi.org/10.1016/j.memsci.2018.12.087.
[30] K.S. Barros, T. Scarazzato, D.C.R. Espinosa, Evaluation of the effect of the solution concentration and membrane morphology on the transport properties of Cu(II) through two monopolar cation–exchange membranes, Sep. Purif. Technol. 193 (2018) 184–192, https://doi.org/10.1016/j.seppur.2017.10.067.
[31] M.C. Martí-Calatayud, D.C. Buzzi, M. García-Gabaldón, A.M. Bernardes, J.A.S. Tenório, V. Pérez-Herranz, Ion transport through homogeneous and heterogeneous ion-exchange membranes in single salt and multicomponent electrolyte solutions, J. Membr. Sci. 466 (2014) 45–57, https://doi.org/10.1016/j.memsci.2014.04.033.
[32] V.V. Nikonenko, N.D. Pismenskaya, E.I. Belova, P. Sistat, P. Huguet, G. Pourcelly, C. Larchet, Intensive current transfer in membrane systems: Modelling, mechanisms and application in electrodialysis, Adv. Colloid Interf. Sci. 160 (2010) 101–123, https://doi.org/10.1016/j.cis.2010.08.001.
[33] C. Larchet, S. Nouri, V. Nikonenko, Application of chronopotentiometry to study the diffusion layer thickness adjacent to an ion-exchange membrane under natural convection, Desalination 200 (2006) 146–148, https://doi.org/10.1016/j.desal.2006.03.276.
[34] E. Belova, G. Lopatkova, N. Pismenskaya, V. Nikonenko, C. Larchet, Role of water splitting in development of electroconvection in ion-exchange membrane systems, Desalination 199 (2006) 59–61, https://doi.org/10.1016/j.desal.2006.03.142.
[35] T. Benvenuti, M. García-Gabaldón, E.M. Ortega, M.A.S. Rodrigues, A.M. Bernardes, V. Pérez-Herranz, J. Zoppas-Ferreira, Influence of the co-ions on the transport of sulfate through anion exchange membranes, J. Membr. Sci. 542 (2017) 320–328, https://doi.org/10.1016/j.memsci.2017.08.021.
[36] N. Pismenskaia, P. Sistat, P. Huguet, V. Nikonenko, G. Pourcelly, Chronopotentiometry applied to the study of ion transfer through anion exchange membranes, J. Membr. Sci. 228 (2004) 65–76, https://doi.org/10.1016/j.memsci.2003.09.012.
[37] E.D. Belashova, N.D. Pismenskaya, V.V. Nikonenko, P. Sistat, G. Pourcelly, Current-voltage characteristic of anion-exchange membrane in monosodium phosphate solution. Modelling and experiment, J. Membr. Sci. 542 (2017) 177–185, https://doi.org/10.1016/j.memsci.2017.08.002.
[38] E.D. Belashova, O.A. Kharchenko, V.V. Sarapulova, V.V. Nikonenko, N.D. Pismenskaya, Effect of protolysis reactions on the shape of chronopotentiograms of a homogeneous anion-exchange membrane in NaH2PO4 solution, Pet. Chem. 57 (2017) 1207–1218, https://doi.org/10.1134/S0965544117130035.
[39] N.D. Pismenskaya, O.A. Rybalkina, A.E. Kozmai, K.A. Tsygurina, E.D. Melnikova, V.V. Nikonenko, Generation of H+ and OH− ions in anion-exchange membrane/ampholyte-containing solution systems: a study using electrochemical impedance spectroscopy, J. Membr. Sci. 601 (2020) 117920, https://doi.org/10.1016/j.memsci.2020.117920.
[40] M.C. Martí-Calatayud, E. Evdochenko, J. Bär, M. García-Gabaldón, M. Wessling, V. Pérez-Herranz, Tracking homogeneous reactions during electrodialysis of organic acids via EIS, J. Membr. Sci. 595 (2020) https://doi.org/10.1016/j.memsci.2019.117592.
[41] V.V. Nikonenko, A.V. Kovalenko, M.K. Urtenov, N.D. Pismenskaya, J. Han, P. Sistat, G. Pourcelly, Desalination at overlimiting currents: state-of-the-art and perspectives, Desalination 342 (2014) 85–106, https://doi.org/10.1016/j.desal.2014.01.008.
[42] O. Rybalkina, K. Tsygurina, E. Melnikova, S. Mareev, I. Moroz, V. Nikonenko, N. Pismenskaya, Partial fluxes of phosphoric acid anions through anion-exchange membranes in the course of NaH2PO4 solution electrodialysis, Int. J. Mol. Sci. 20 (2019) https://doi.org/10.3390/ijms20143593.
[43] M.C. Martí-Calatayud, M. García-Gabaldón, V. Pérez-Herranz, Mass transfer phenomena during electrodialysis of multivalent ions: chemical equilibria and overlimiting currents, Appl. Sci. 8 (2018) 1566, https://doi.org/10.3390/app8091566.
[44] F.Q. Mir, A. Shukla, Sharp decline in counter-ion transport number of electrodialysis ion exchange membrane on moderate increase in temperature, Desalination 372 (2015) 1–6, https://doi.org/10.1016/j.desal.2015.06.009.
[45] S.A. Mareev, D.Y. Butylskii, N.D. Pismenskaya, V.V. Nikonenko, Chronopotentiometry of ion-exchange membranes in the overlimiting current range. Transition time for a finite-length diffusion layer: modeling and experiment, J. Membr. Sci. 500 (2016) 171–179, https://doi.org/10.1016/j.memsci.2015.11.026.
[46] K.J. Vetter, Electrochemical Kinetics: Theoretical and Experimental Aspects, Acad. Press, New York, 1967.
[47] H.J.S. Sand, On the concentration at the electrodes in a solution, with special reference to the liberation of hydrogen by electrolysis of a mixture of copper sulphate and sulphuric acid, J. London, Edinburgh, Dublin Philos, Mag. J. Sci. 17 (1899) https://doi.org/10.1016/0302-4598(75)85003-3.
[48] M. García-Gabaldón, V. Pérez-Herranz, E. Ortega, Evaluation of two ion-exchange membranes for the transport of tin in the presence of hydrochloric acid, J. Membr. Sci. 371 (2011) 65–74, https://doi.org/10.1016/j.memsci.2011.01.015.
[49] V.V. Nikonenko, N.D. Pismenskaya, E.I. Belova, P. Sistat, P. Huguet, G. Pourcelly, C. Larchet, Intensive current transfer in membrane systems: modelling, mechanisms and application in electrodialysis, Adv. Colloid Interf. Sci. 160 (2010) 101–123, https://doi.org/10.1016/j.cis.2010.08.001.
[50] M.K. Urtenov, A.M. Uzdenova, A.V. Kovalenko, V.V. Nikonenko, N.D. Pismenskaya, V.I. Vasil'eva, P. Sistat, G. Pourcelly, Basic mathematical model of overlimiting transfer enhanced by electroconvection in flow-through electrodialysis membrane cells, J. Membr. Sci. 447 (2013) 190–202, https://doi.org/10.1016/j.memsci.2013.07.033.
[51] E. Volodina, N. Pismenskaya, V. Nikonenko, C. Larchet, G. Pourcelly, Ion transfer across ion-exchange membranes with homogeneous and heterogeneous surfaces, J. Colloid Interface Sci. 285 (2005) 247–258, https://doi.org/10.1016/j.jcis.2004.11.017.
[52] M. Wang, X. Liang Wang, Y. Xiang Jia, X. Liu, An attempt for improving electrodialytic transport properties of a heterogeneous anion exchange membrane, Desalination 351 (2014) 163–170, https://doi.org/10.1016/j.desal.2014.07.039.
[53] M.C. Martí-Calatayud, M. García-Gabaldón, V. Pérez-Herranz, E. Ortega, Determination of transport properties of Ni(II) through a Nafion cation-exchange membrane in chromic acid solutions, J. Membr. Sci. 379 (2011) 449–458, https://doi.org/10.1016/j.memsci.2011.06.014.